RSC Advances

PAPER

View Article Online
View Journal | View Issue

Cite this: *RSC Adv.*, 2023, **13**, 24423

Colorless and transparent poly(amide imide) nanocomposites containing organically modified hectorite

A Young Kim,[a] Seon Ju Lee,[a] Moon Young Choi,[a] Changyub Na,[a] Lee Ku Kwac,[ab] Hong Gun Kim[ab] and Jin-Hae Chang *[b]

Received 10th July 2023
Accepted 2nd August 2023

DOI: 10.1039/d3ra04587k

rsc.li/rsc-advances

Polyamic acid (PAA) was synthesized using the diamine monomer *N*,*N*′-[2,2′-bis(trifluoromethyl)-4,4′-biphenylene]bis(4-aminobenzamide) and dianhydride monomer 4,4′-oxydiphthalic anhydride. Colorless and transparent poly(amide imide) (CPAI) hybrid films were prepared *via* multi-step thermal imidization of PAA in which various contents of nano-filler were dispersed. The CPAI hybrid films were prepared by dispersing organoclay STN, which was obtained by organically modifying hectorite, in CPAI by solution intercalation with various contents ranging from 1 to 7 wt%. The thermomechanical properties, morphologies, and optical transparencies of the obtained CPAI hybrid films were investigated based on the dispersed STN content, and the results were compared. Some of the clay in the CPAI hybrid film were agglomerated, which was observed using a transmission electron microscope; however, most clays were well-dispersed, with a nano-size of less than 10 nm. The best thermomechanical properties of the CPAI hybrid film were exhibited with an STN content of 3 wt%, but these properties decreased above the critical content. The coefficients of thermal expansion of all the hybrid films were below 20 ppm per °C regardless of the amount of STN, and the yellow index was 1–2 even when the STN content increased to 7 wt%.

1. Introduction

Polyimide (PI), a super-engineered plastic, is a polymer with an imide ring in the main chain and a mostly amorphous structure.[1,2] PI is a polymer material with excellent heat resistance, chemical resistance, and mechanical properties because of the strong chain structure of imide-based aromatics and the π–π interaction between chains.[3,4] Since the 1980s, the scope of PI has greatly expanded and has been used as a core material in coatings for automobiles and airplanes, alignment films for liquid-crystal displays, and flexible printed circuit boards.[5–7] Recently, PI has been used in semiconductors and electronic materials because it is lightweight and precise. However, conventional PIs have poor processability because they are insoluble or infusible, and their use in transparent displays is limited because of the inherent dark brown color.[8,9]

PI is known to exhibit a dark brown color because of the charge transfer complex (CTC) effect that occurs between (intermolecular) or within (intra-molecular) the molecules of the PI polymer chain.[10,11] In order to block the charge transfer complex (CTC) that appears in aromatic PI and synthesize colorless and transparent PI (CPI), the following method is mainly used: (1) introducing functional groups:[12] by incorporating functional groups such as trifluoromethyl (–CF_3), sulfone (–SO_2–), and ether (–O–), which possess strong electronegativity, into the main chain of the polyimide, the movement of π electrons in the chain is restricted. These electronegative groups can disrupt the formation of CTCs and reduce their impact on the optical properties of the polymer. (2) *Meta*-substituted monomer structure:[13] the introduction of a *meta*-substituted monomer structure in the main chain of the polyimide leads to bending of the entire polymer structure. This structural modification helps prevent the movement of π electrons along the chain, further minimizing the formation of CTCs. The *meta*-substituted configuration disrupts the extended conjugation, reducing the likelihood of charge transfer interactions. (3) Introducing alicyclic monomers:[14] recently, the use of alicyclic monomers has been explored to improve the properties of polyimides. The incorporation of alicyclo-ring structures into the monomer units can significantly reduce the occurrence of CTCs. The presence of alicyclic rings interrupts the extended conjugation in the polymer backbone, which mitigates the formation of CTCs and enhances the transparency of the resulting CPI films. These strategies collectively aim to limit the movement of π electrons, disrupt extended conjugation, and reduce the occurrence of CTCs, thereby improving the transparency and colorlessness of polyimide films.

[a]*Graduate School of Carbon Convergence Engineering, Jeonju University, Jeonju 55069, Korea*

[b]*Institute of Carbon Technology, Jeonju University, Jeonju 55069, Korea. E-mail: jhchang@jj.ac.kr*

Colorless and transparent PI (CPI) has better optical properties than conventional PI; however, it exhibits poor thermomechanical properties. This finding can be explained by the fact that the bent structure or the highly electronegative substituent introduced into the main chain of the CPI to improve the optical properties deteriorates the thermomechanical properties. These disadvantages can be overcome by developing new monomers to improve the thermomechanical properties while partially maintaining the transparency of CPI. Studies on copolyimide have been conducted to improve the thermomechanical properties even at low transparency by partially using a monomer with a rigid-type structure.

The poor processability and low solubility because of the aromatic structure and rigid main chain used in PI can be improved by significantly overcoming the disadvantages of PI by employing structures such as esters, ethers, amides, and sulfones in the imide structure.[15–17] Among these, poly(amide imide) (PAI), which contains an amide group in the PI main chain, exhibits high thermal stability and improved mechanical properties because of the synergistic effect of polyamide and PI. In addition, compared to other PIs, PAI exhibits better thermal properties owing to the hydrogen bonding between the amide chains and good solubility in amide-based polar solvents. Because of these advantages, PAI is used in various applications, including wire enamel, adhesives, membrane, injection, extrusion products, and other electronic devices.[18–20]

Based on the research studies, for CPI to have good thermal and mechanical properties, straight and rigid monomers must be used to ensure the CPI main chain has a rigid structure. The colorless transparency of CPI can be maintained by introducing an anhydride or amine moiety with an overall bent structure. Conversely, CPIs containing the *meta*-structures have poor thermal and mechanical properties compared to those containing *para*-structures. For example, CPIs synthesized using 4,4′-(hexafluoroisopropylidene) diphthalic anhydride (6FDA) monomers have excellent optical properties because of the high electronegativity of $-CF_3$ substituent; however, they have low thermal stability because of the weak thermal effect of the $-CF_3$ substituent.[21,22] These findings indicate that the colorless transparency and thermal properties of CPI are inversely proportional. Many studies have been conducted on linear and rigid monomers that maintain a certain degree of transparency without deteriorating the thermal and mechanical properties of CPI to compensate for these disadvantages.[23,24]

In a recent paper, Wu *et al.*[25] presented results on PI showing high transparency and colorlessness using rigid linear monomers. A method for synthesizing CPI without using the previously used bent structure and strong electron attraction is introduced. In addition, CPI with a high glass transition temperature (T_g) was also synthesized using structures of aromatic monomers and alicyclic monomers containing small substituents.

Polymer nanocomposites obtained by exfoliating fillers, such as clay, graphene, carbon nanotubes, layered double hydroxides (LDHs), and polyhedral oligomeric silsesquioxanes (POSS) with a nanosized layered structure, from matrix polymers offer several advantages and exhibit various physical properties compared to simple blended general composites. These effects can be attributed to the unique characteristics of nanoscale fillers and their interaction with the polymer matrix, resulting in improved mechanical, thermal, barrier, electrical, and optical properties of the nanocomposites compared to simple blended composites.[26–28]

Especially, clay-based nanocomposites overcome the limitations of various physical properties that cannot be seen in traditional composites, and show synergistic effects of multifunctionality and high performance. Most clays used as fillers consist of layered silicate structures. Common smectite-based clays include montmorillonite (MMT), saponite, hectorite, bentonite, and mica.[29]

Pristine clay has poor dispersibility and compatibility with the polymer matrix. Hence, an organically modification reaction is performed on the clay surface to overcome these disadvantages. Because hectorite clay is hydrophilic and incompatible with lipophilic CPI polymers, its surface must be modified with an appropriate organic material to increase its dispersibility.[30,31] STN is a hectorite-based organoclay that can be effectively dispersed in a matrix to improve the physical properties of CPI hybrids significantly. STN is widely used as a reinforcing material for polymer matrices because of its heat resistance and excellent electrical and mechanical properties.[32–34]

In the meantime, many papers on PAI nanocomposites using various types of nano fillers have been published. In particular, in the case of using clay, a change in physical properties was observed depending on the degree of dispersion and the content of the filler, and the physical properties were improved even with a small amount of less than 3%.[35,36] In order to develop a substrate suitable for a flexible display, a flexible material capable of continuous processing is essential instead of glass, but when using a general polymer, it is very difficult to apply in practice due to low heat resistance. In addition, conventionally developed PAIs have excellent heat resistance but have low optical properties, making it difficult to apply them to flexible display substrates. If a PAI nanocomposite that can improve the high heat resistance and optical properties of PAI is developed using a small amount of nano filler, it can be widely used in various electronic materials including the flexible display field.[37,38]

When using monomers frequently used for CPI, the poor thermal properties of CPI can be slightly improved; however, improving the original low CPI thermal properties is limited. Therefore, synthesizing special monomers with better thermomechanical properties while maintaining the existing optical transparency is essential. In this study, when a colorless and transparent PAI (CPAI) film was prepared by introducing an amide group into a monomer containing $-CF_3$; the thermomechanical properties were expected to be improved *via* hydrogen bonding between the chains in CPAI.[39,40] Simultaneously, an amine monomer of *N*,*N*′-2,2′-bis(trifluoromethyl)-4,4′-biphenylene-bis (4-aminobenzamide) (TFAB) containing 2,2′-bis(trifluoro-methyl) benzidine (TFB) moiety was directly synthesized to improve thermomechanical properties while maintaining the optical transparency of existing CPAI.[37] In

addition, because the amide functional group present in TFAB can form hydrogen bonds with the hydrophilic clay, it significantly affects the clay dispersion in the matrix.

In this study, various STN contents were dispersed in polyamic acid (PAA), synthesized using TFAB containing an amide group and 4,4′-oxydiphthalic anhydride (ODPA) containing a *meta*-substituted ether group, and CPAI hybrid films were prepared *via* several stages of heat treatment. The thermomechanical properties, morphologies, and optical transparencies of the CPAI hybrid films with different STN contents have been described, and the results have been compared.

2. Experimental

2.1 Materials

All reagents for synthesizing CPAI were purchased from Aldrich Chemical Co. (Yongin, Korea). *N*,*N*′-Dimethylacetamide (DMAc) was mixed with a molecular sieve (4 Å) for a long time to remove moisture altogether before use. Pristine hectorite and STN was purchased from CO-OP Chem. (Tokyo, Japan). STN is an organoclay obtained through an organic reaction on the surface of hectorite-based clay. The cation exchange capacity of hectorite is 78 meq/100 g. Hectorite is composed of stacked silicate sheets. The layer thickness of each sheet was 1 nm, and the axial ratio (length/diameter, *L*/*D*) was approximately 46.[41]

2.2 Synthesis of TFAB

TFAB was synthesized using a multistep method, according to our previously published method.[37]

2.3 Synthesis of CPAI hybrid films using STN

CPAI hybrid films were obtained *via* a two-step synthesis method. The detailed synthesis method is as follows: TFAB (10.34 g, 1.85×10^{-2} mol) was dissolved in DMAc (30 mL) and stirred at 0 °C for 1 h under nitrogen. A solution of ODPA (5.74 g; 1.85×10^{-2} mol) in DMAc (40 mL) was added to the TFAB/DMAc solution. The resulting mixture was vigorously stirred at 25 °C for 14 h to obtain a PAA solution.

The method for synthesizing CPAI hybrid films with various organoclay contents was the same; the synthesis of CPAI hybrid film containing 3 wt% STN has been demonstrated as an example. STN (0.064 g) and PAA solution (13.0 g) were added to DMAc (20 mL), and the mixture was vigorously stirred at 25 °C for 14 h. The solution was reacted with an ultrasonic cleaner for 3 h and dried in a vacuum oven at 50 °C for 30 min and 80 °C for 1 h to remove the solvent altogether. Finally, the PAA film was sequentially heat-treated at each temperature from 110 to 235 °C on a glass plate to obtain a CPAI hybrid film. The detailed heat-treatment conditions are listed in Table 1. The thickness of the final hybrid film obtained by heat treatment was approximately 10–12 μm regardless of the STN content. The synthesis route for the CPAI hybrid film and the chemical structures of the compounds are shown in Scheme 1. The solution viscosity of the PAI films obtained from PAA under various heat treatment conditions was measured using DMAc. Inherent viscosity (η_{inh}) was 0.86 dL g^{-1}.

Table 1 Heat-treatment conditions of CPAI hybrid films

Samples	Temperature (°C)/time (h)/pressure (Torr)
PAA	25/14/760 → 50/0.5/1 → 80/1/1
CPAI hybrid	110/0.5/1 → 140/0.5/1 → 170/0.5/1 → 195/1/1 → 220/1/1 → 235/2/1

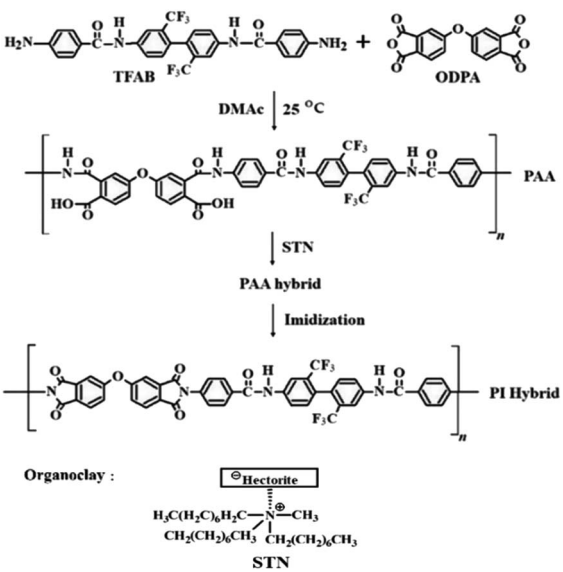

Scheme 1 Synthesis route for the fabrication of CPAI hybrid films.

An attempt was made to investigate the physical properties by obtaining a CPAI hybrid film with an STN of 9 wt% or more. When an excessive amount of STN was added, the viscosity of PAA increased rapidly, and the clay agglomerated and was improperly dispersed.

2.4 Characterizations

To confirm the structure of the synthesized CPAI hybrid film, we employed Fourier transform infrared (FT-IR; PerkinElmer, Spectrum Two, Lantrisant, UK) and solid-state ^{13}C cross-polarized magic angle spinning nuclear magnetic resonance (^{13}C MAS NMR; Bruker 400 DSX NMR, Berlin, Germany) spectroscopy. NMR chemical shifts were based on the tetramethylsilane peak.

The results of wide-angle X-ray diffraction (XRD; PANalytical X'Pert PRO MRD, Amsterdam, Netherlands) were obtained using a Cu-Kα target equipped with a Ni filter. The 2θ range was 2–15°, and the scan speed was 2° min^{-1}. Transmission electron microscopy (TEM; EM 912 Omega, Carl Zeiss, Berlin, Germany) was used to measure clay dispersion in the hybrid film. The samples cured with epoxy were cut to a thickness of 90 nm using a microtome.

To investigate the thermal properties of pure CPAI and CPAI hybrid films, we employed differential scanning calorimetry (DSC; DuPont 910, New York, USA) and thermogravimetric analysis (TGA, TA instruments Q500, New Castle, DE, USA) under a nitrogen stream at a heating rate of 20 °C min^{-1}. A

thermomechanical analyzer (TMA; SS6100, Tokyo, Japan) was used to determine the coefficient of thermal expansion (CTE) of the hybrid films with different clay contents. The size of the film was 30 mm × 5 mm, and the heating rate and applied force were 5 °C min^{-1} and 0.1 N, respectively. In order to obtain reliable results, the CTE was determined by performing the first heating at 50 to 200 °C and then the second heating at the same temperature condition.

The tensile properties of the hybrid films obtained by casting were measured using a universal testing machine (Instron Model 5564, New York, NY, USA) at room temperature and a crosshead speed of 20 mm min^{-1}. Experimental errors in tensile strength and tensile modulus were ±1 MPa and ±0.05 GPa, respectively. To obtain an accurate value, we tested each sample at least 10 times; the lowest and highest values were discarded, and the rest were averaged.

The optical transmittance was investigated by measuring the cut-off wavelength (λ_o) and transmittance at 500 nm (500 nm^{trans}) using an ultraviolet-visible spectrophotometer (UV-vis; SHIMADZU UV-3600, Tokyo, Japan). The yellow index (YI) was determined using a spectrophotometer (Konica Minolta, CM-3600d, Tokyo, Japan).

3. Results and discussion

3.1 FT-IR and ^{13}C-solid state NMR

Fig. 1 shows the FT-IR spectra of the synthesized CPAI films. The C=O asymmetric and symmetric stretching peaks were observed at 1777 cm^{-1} and 1714 cm^{-1}, respectively. The characteristic C–N–C peak at 1364 cm^{-1} indicated the successful synthesis of CPAI.[42]

Structural analysis of the synthesized PI was performed using solid-state ^{13}C MAS NMR spectroscopy. The ^{13}C chemical shifts at room temperature are shown in Fig. 2. In the NMR spectrum, the peaks at 141.06, 130.13, and 119.31 ppm were assigned to the phenyl carbons (a–c and e). The ^{13}C chemical shift for $-CF_3$ was observed at 130.13 ppm (d). The chemical shifts for the amide C=O and imide C=O were observed at 161.66 ppm (f) and 168.11 ppm (g), respectively.[43] The spinning sidebands for the phenyl group are marked with asterisks in

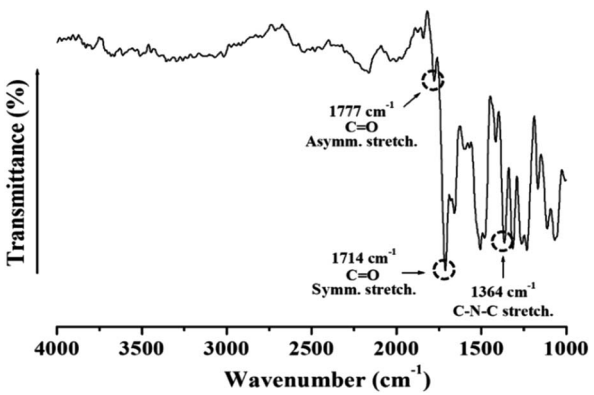

Fig. 1 FT-IR spectrum of CPAI.

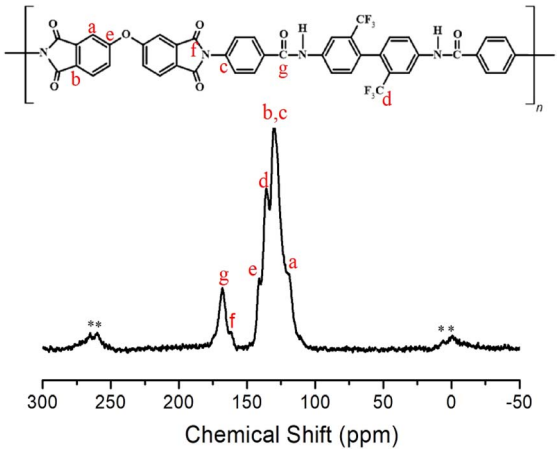

Fig. 2 ^{13}C-NMR spectrum of CPAI.

Fig. 2. The chemical structure of the synthesized CPAI was confirmed using IR and NMR.

3.2 XRD

Fig. 3 shows the XRD patterns of pristine clay (hectorite), STN with organic functional groups formed *via* a cation–exchange reaction, and CPAI hybrid films with various STN contents. The characteristic peak of hectorite appeared at $2\theta = 6.58°$ (d = 13.42 Å), and that for STN, obtained by the organic reaction of hectorite, appeared at $2\theta = 4.60°$ (d = 19.19 Å). The interlayer distance in STN, obtained by organically treating pristine clay with an alkyl group, increased by 5.77 Å compared to that in pristine clay. The widened interlayer spacing facilitates the intercalation of the polymer chains and can further increase the degree of dispersion.[44] As shown in Fig. 3, no peak was observed even when the STN content was increased to 5 wt%. This result means that even when 5 wt% of the filler was added, it was completely dispersed in the CPAI matrix at the nano level. While XRD analysis can provide information about the structural characteristics of materials, including the degree of order or crystallinity, it may not provide direct evidence of exfoliation in the case of polymeric materials. To confirm whether the obtained results indicate exfoliation, further characterization techniques such as TEM should be employed. However, when the STN content reached 7 wt%, a very weak intensity peak appeared at $2\theta = 5.50°$ (d = 16.05 Å). These results were obtained because the clay was not well dispersed in the CPAI matrix and agglomerated as the clay content increased.[45,46]

XRD is the simplest device for confirming the agglomeration of clays dispersed in a hybrid and measuring the distance between clay layers; however, it has only a one-dimensional resolution.[47] To obtain more detailed information about the dispersion, observing and confirming the detailed morphology of the clay dispersed in the matrix using TEM was necessary.

3.3 Morphology of hybrid film using TEM

Using TEM, the actual interlayer structure of the dispersed clay can be quantitatively determined, as well as its good dispersion,

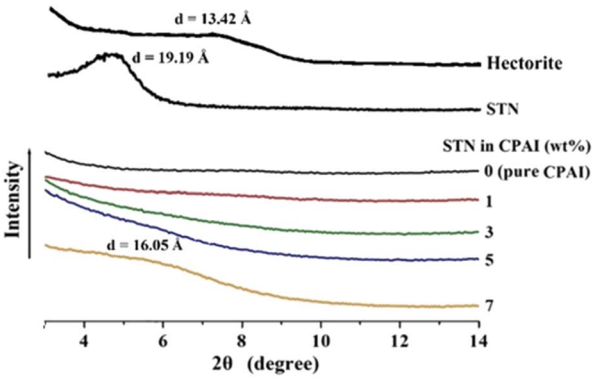

Fig. 3 XRD patterns of pristine clay, organoclay, and CPAI hybrids films containing various organoclay contents.

at the nanoscale in the CPAI matrix. Accurate information about the nanocomposite was obtained, complementing the XRD results. Fig. 4 shows TEM images of hybrid films containing 3, 5, and 7 wt% of STN that were obtained to observe the dispersion of clay in the CPAI matrix. Hair-like black lines are observed in each image, representing 1 nm-thick clay layers, and the space between them represents the spacing between the clay layers. In addition, the area indicated by the arrow was enlarged according to the magnification to observe a more detailed dispersion.

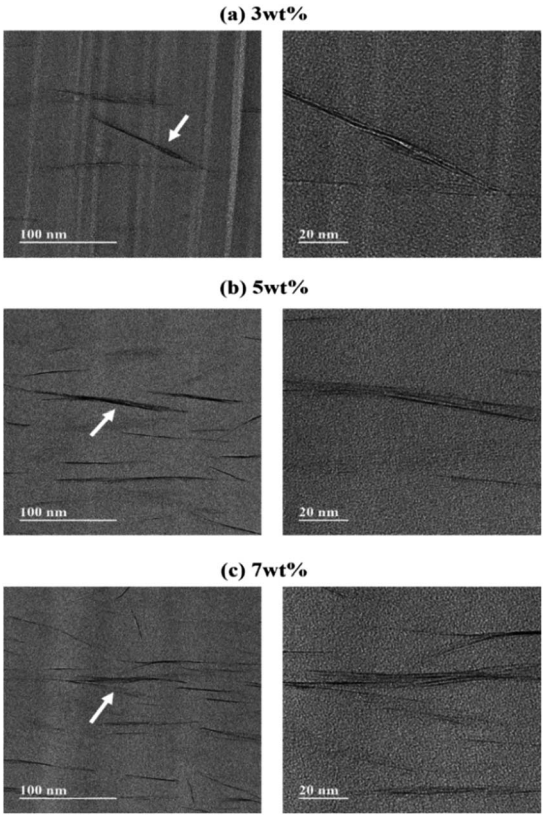

Fig. 4 TEM images of CPAI hybrid films containing (a) 3, (b) 5, and (c) 7 wt% STN (images recorded under different magnification conditions).

When the organoclay contents were 3 and 5 wt% (Fig. 4a and b), it was well dispersed with a thickness of less than 10 nm. When the STN content increased to 7 wt% (Fig. 4c), the clay aggregated more than that at low STN contents. The XRD results in Fig. 3 also confirmed these findings. Although the clay aggregated as the STN content increased from 1 to 7 wt%, nano-size hybrids in which the clay was well dispersed with an average thickness of less than 20 nm were formed in the CPAI matrix. In particular, STN was best dispersed, with a thickness of less than 10 nm, at a content of 3 wt%. As discussed later, this was a positive factor for the thermomechanical properties.

3.4 Thermal property

The T_g of polymers varies depending on the chain mobility, free volume, structural differences, curing reactions, chemical bonding (such as hydrogen bonding), and the presence of additives.[48,49] Aromatic PI-based polymers usually have a high T_g because of their poor fluidity. In this study, although a *meta*-substituted ODPA structure lowers the thermal stability, a high T_g is expected because of the difficulty in movement owing to the presence of many aromatic structures in the diamine structure (TFAB). Table 2 lists the thermal properties of CPAI hybrids with various STN contents. As the STN content in the CPAI hybrid film increased from 0 to 3 wt%, the T_g increased continuously from 221 to 242 °C. This finding can be explained by the fact that the clay was evenly dispersed in the matrix polymer, which changed the free volume of the polymer chain between the clay layers and impeded the segmental movement. In addition, the T_g increased because the movement of the polymer chains, evenly dispersed in the clay, was hindered by the hydrogen bonding of the amide group of the TFAB moiety.[50]

However, when the STN content increased to 7 wt%, the T_g suddenly decreased to 214 °C. The result is that the clay added to the hybrid does not disperse effectively above a certain critical content and rather reduces the T_g value.[51] The result was also cross-checked with the XRD and TEM results (Fig. 3 and 4). DSC thermograms of the CPAI hybrids with various STN contents are shown in Fig. 5.

The TGA results for the hybrid films are presented in Table 2. The initial decomposition temperature (T_D^i) increased from 452 to 463 °C as the STN content increased from 0 to 3 wt%. This finding can be explained by the fact that up to 3 wt% of clay was well dispersed in the matrix polymer, suppressing the thermal

Table 2 Thermal properties of CPAI hybrid films containing various organoclay contents

STN in CPAI (wt%)	T_g (°C)	T_D^i[a] (°C)	wt_R^{600}[b] (%)	CTE[c] (ppm per °C)
0 (pure CPAI)	221	452	69	16.4
1	233	458	69	14.9
3	242	463	71	14.0
5	238	431	70	15.9
7	214	400	68	16.6

[a] Initial decomposition temperature at 5% weight loss. [b] Weight residue at 600 °C. [c] Coefficient of thermal expansion for 2nd heating is 50–200 °C.

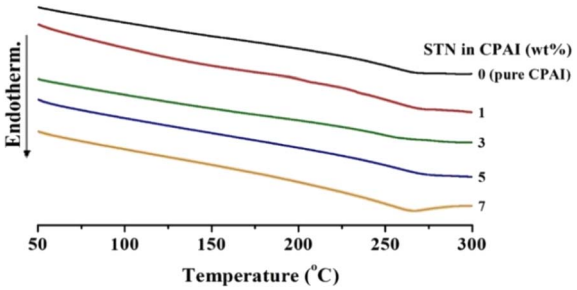

Fig. 5 DSC thermograms of CPAI hybrid films containing various organoclay contents.

decomposition of the polymer intercalated between the clay layers and simultaneously preventing the outflow of volatilized components into the gas.[52,53] However, as the content of the filler increased from 3 to 7 wt%, the effect of inhibiting thermal decomposition was not observed because of the agglomeration of the clay. Hence, the (T_D^i) decreased to 400 °C. This value is also lower than that of pure CPAI (452 °C). This result is because the excessive clay dispersed in the matrix did not effectively block heat due to aggregation and also did not suppress volatile substances generated during heating at high temperatures. Because using fillers above the critical content reduces their effect, selecting the critical content and type of filler in hybrids is crucial. The residual weight of the hybrid, when heated at 600 °C (wt_R^{600}), was also the highest (71%) when the STN content was 3 wt%; however, no significant difference was observed compared to other hybrids (68–70%). This result may be influenced by the Hofmann decomposition of ammonium, which modifies cations in hectorite.[54] This modification of cations in hectorite leads to the formation of acid sites within the clay structure. These acid sites can then act as catalysts for the decomposition of the polymer matrix.

Fig. 6 shows the TGA thermograms of CPAI hybrids with various STN contents. A slight decomposition of 1–2% was observed at approximately 250 °C before major decomposition occurred. This decomposition occurred because an alkyl group with weak thermal stability was substituted into the organoclay STN.

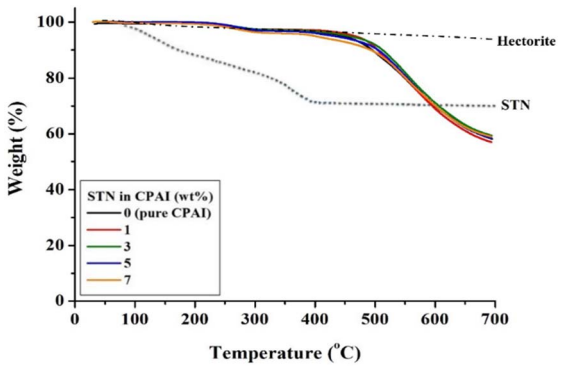

Fig. 6 TGA thermograms of CPAI hybrid films containing various organoclay contents.

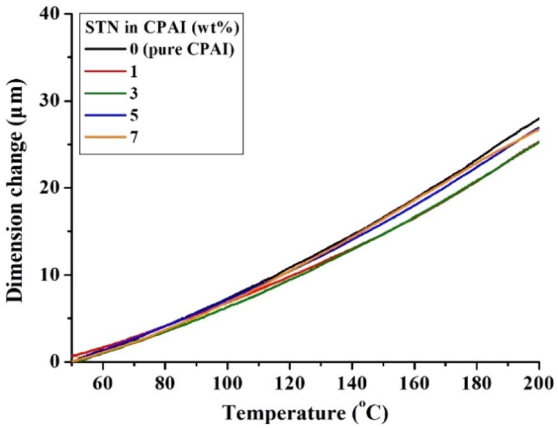

Fig. 7 TMA thermograms of CPAI hybrid films containing various organoclay contents.

When a polymer is heated, it expands perpendicular to its main chain. However, the thermal expansion of polymers becomes difficult if heat is not transferred to the polymer chains between the wide plate-shaped clays with high heat resistance. Consequently, clays with high thermal stability and an appropriate reduction in heat transfer can suppress the thermal expansion of polymers.[55,56] Table 2 summarizes the CTE values of CPAI hybrid films with various STN contents obtained after secondary heating between 50 and 200 °C. The lowest CTE value of 14.0 ppm per °C was obtained when the critical STN content was 3 wt%. The CTE value did not change significantly in the range of 14.0 to 16.6 ppm per °C depending on the STN content and showed relatively excellent values compared to other CPI hybrids. Fig. 7 shows the TMA results for the CPAI hybrid films with various STN contents.

These results also indicate that the thermal stability of the clay plate, made of inorganic materials, is high, and the overall thermal properties (T_g, (T_D^i), and CTE) increased because the insulating effect of the dispersed clay in the CPAI matrix hindered heat transfer. However, the thermal properties deteriorated when the organoclay content exceeded the critical value. This finding can be explained by the fact that the clay was not well dispersed in the matrix and agglomerates, reducing the compatibility and producing a poor heat shielding effect.

3.5 Mechanical property

Table 3 summarizes the tensile mechanical properties of the CPAI hybrid films based on the amount of STN dispersion. The tensile strength increased slightly from 55 to 62 MPa as the STN content increased from 0 to 1 wt%. This value increased to 81 MPa when the amount of STN increased to 3 wt%. However, when the organoclay content was increased from 3 to 7 wt%, the tensile strength gradually decreased to 65 MPa. This phenomenon has previously been reported in several studies and can be explained based on the fact that excess clay above the critical content does not disperse relatively effectively and agglomerates compared to lower content.[57,58]

A similar trend was observed for the modulus (Table 3). As organoclay content increased from 0 to 3 wt%, the modulus

Table 3 Mechanical properties of CPAI hybrid films containing various organoclay contents

STN in CPAI (wt%)	Ult. str.[a] (MPa)	Ini. mod.[b] (GPa)	EB[c] (%)
0 (pure CPAI)	55	4.19	23
1	62	5.98	19
3	81	7.12	18
5	74	6.03	15
7	65	5.88	15

[a] Ultimate strength. [b] Initial modulus. [c] Elongation at break.

increased from 4.19 to 7.12 GPa. The rigidity of the clay and the constant orientation of clay with a large aspect ratio can explain this increase in the modulus. Moreover, the difficulty in deforming the main oriented chain of the polymer intercalated between the clays may have also contributed to the increase in the modulus. However, similar to the tensile strength results, when the STN content increased to 7 wt%, the modulus decreased to 5.88 GPa. Compared with the CPI obtained using TFB, the CPAI obtained using TFAB showed a much higher value. This higher value is because the amide and phenyl groups in the rigid-type structure of the TFAB moiety make it more rigid than the TFB monomer, and the attraction between the polymer chains is significant. The mechanical properties were directly affected by the content and orientation of the dispersed clay, and clay above a critical content exhibited the opposite effect of degrading the mechanical properties of the hybrid.

The elongation at break (EB) of the CPAI hybrids decreased as the STN content increased. EB for pure CPAI was 23%; however, it slowly decreased from 19 to 15% as the STN content increased from 1 to 7% (Table 3). This difference is due to the inherent properties of inorganic clays, such as brittleness and inelasticity, as well as the presence of nanofiller sheets that influence crack generation and propagation in composites.

3.6 Optical transparency

The optical transparency of the CPAI hybrid film can be explained based on the results of λ_o, 500 nm^{trans}, and YI. The results obtained using a UV-vis spectrophotometer are listed in Table 4. The λ_o values of all CPAI hybrid films, regardless of the STN content, were approximately 370 nm, less than 400 nm in the visible region. These low λ_o values are significantly superior to those published for various CPIs thus far and show very high commercial applicability. In addition, the maximum 500 nm^{trans} of the CPAI hybrid films showed a constant value (82–85%), although it slightly decreased as the STN content increased. Fig. 8 shows the UV-vis spectroscopy results of CPAI hybrid films with various STN contents. These results indicate that the clay dispersed evenly in an almost exfoliated state in the CPAI matrix had a slight effect on the light transmittance (Fig. 4). Table 4 summarizes the YI values of the various CPAI hybrid films based on STN content. The YI values of the hybrid films were constant, regardless of the STN content, and showed very low values of YI = 1–2. These values indicate an almost colorless and transparent film with a YI value similar to that of poly(methyl methacrylate) (YI = 1–2),[59] which was used as a substitute for glass long ago.

A photograph of the film using the logo is shown in Fig. 9 to visually verify the degree of colorless transparency of the hybrid films. Regardless of the STN content, the letters or pictures of the logo seen through all the hybrid films were clearly visible, and no difference was observed in sharpness with the differing filler content.

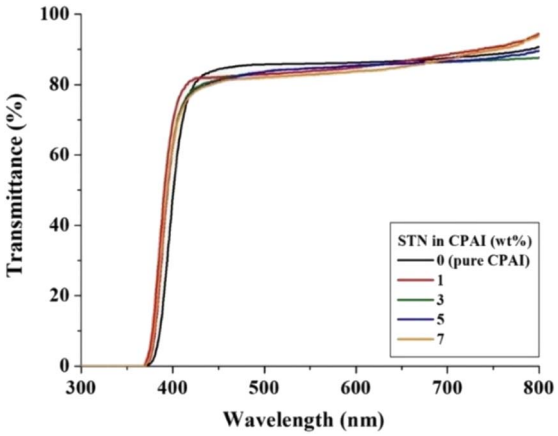

Fig. 8 UV-vis transmittance of CPAI hybrid films containing various organoclay contents.

Table 4 Optical transparencies of CPAI hybrid films containing various organoclay contents

STN in CPAI (wt%)	Thickness[a] (μm)	λ_o[b] (nm)	500 nm^{trans} (%)	YI[c]
0 (pure CPAI)	10	370	85	1
1	10	369	85	1
3	11	370	83	1
5	11	370	83	2
7	12	370	82	2

[a] Film thickness. [b] Cut off wavelength. [c] Yellow index.

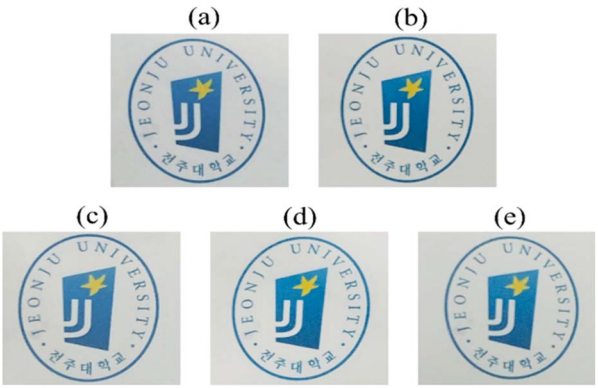

Fig. 9 Photographs of CPAI hybrid films containing various organoclay contents. (a) 0 (pure CPAI), (b) 1, (c) 3, (d) 5, and (e) 7 wt% of STN.

4. Conclusions

The effects of various clay contents on the physical properties of the hybrids produced by dispersing nanosized clay in a polymer matrix were studied. CPAI was synthesized using the diamine TFAB and dianhydride ODPA and organically modified clay, STN, was used for synthesizing the CPAI hybrid film. The STN content of the CPAI hybrid films varied from 1 to 7 wt%.

The thermomechanical properties were the best when STN was dispersed at a critical content of 3 wt%. When the organoclay content was excessively dispersed, the clay agglomeration deteriorated all physical properties. Overall, even a small amount of STN dispersion effectively improved the thermomechanical properties of the CPAI hybrid film while maintaining optical transparency. All the prepared hybrid films were colorless and transparent, regardless of the amount of clay added, and their optical properties were similar to glass.

The CPAI obtained in this study can be widely used for various applications that require high-performance plastics because of its excellent thermomechanical properties and optical transparency if further research in various fields is supplemented. In addition, if the monomer structure and type of filler constituting the CPAI hybrid film are appropriately selected, excellent physical properties can be obtained, and the application field can be expanded.

Author contributions

J.-H. Chang designed the project and wrote the manuscript. L. K. Kwac and H. G. Kim reviewed and analyzed the data. A. Y. Kim, S. J. Lee, M. Y. Choi, and C. Na prepared the samples and participated in the data analysis. All authors have read and agreed to the published version of the manuscript.

Conflicts of interest

The authors declare no conflict of interest.

Acknowledgements

This research was supported by the Basic Science Research Program through the National Research Foundation of Korea (NRF) funded by the Ministry of Education (2016R1A6A1A03012069). This work also was supported by the National Research Foundation of Korea (NRF) grant funded the Korea government (MSIT) (2022R1A2C1009863).

References

1 C. P. Feng, L. Bai, R.-Y. Bao, S.-W. Wang, Z. Liu, M.-B. Yang, J. Chen and W. Yang, *Compos. Commun.*, 2019, **12**, 80–85.
2 Li. Gouzman, E. Grossnab, R. Verker, N. Atar, A. Bolker and N. Eliaz, *Adv. Mater.*, 2019, **31**, 1807738–1807752.
3 D.-J. Liaw, K.-L. Wang, Y.-C. Huang, K.-R. Lee, J.-Y. Lai and C.-S. Ha, *Prog. Polym. Sci.*, 2012, **37**, 907–974.
4 J. S. Ho and S. G. Greenbaum, *ACS Appl. Mater. Interfaces*, 2018, **10**, 29189–29218.
5 M.-C. Choi, Y. Kim and C.-S. Ha, *Prog. Polym. Sci.*, 2008, **33**, 581–630.
6 P. E. Burrows, G. L. Graft, M. E. Gross, P. M. Martin, M. K. Shi, M. Hall, E. Mast, C. Bonham, W. Bennett and M. B. Sullivan, *Displays*, 2001, **22**, 65–69.
7 C.-J. Chiang, C. Winscom, S. Bull and A. Monkman, *Org. Electron.*, 2009, **10**, 1268–1274.
8 K.-I. Fukukawa and M. Ueda, *Polym. J.*, 2008, **40**, 281–296.
9 H. R. Khaleel, H. M. Al-Rizzo and D. G. Rucker, *J. Disp. Technol.*, 2012, **8**, 91–97.
10 C.-J. Chen, H.-J. Yen, Y.-C. Hu and G.-S. Liou, *J. Mater. Chem. C*, 2013, **1**, 7623–7634.
11 M. Nishihara, L. Christiani, A. Staykov and K. Sasaki, *J. Polym. Sci., Part B: Polym. Phys.*, 2014, **52**, 293–298.
12 M. Hasegawa, Y. Hoshino, N. Katsura and J. Ishii, *Polymer*, 2017, **111**, 91–102.
13 H. Ni, J. Liu, Z. Wang and S. Yang, *J. Ind. Eng. Chem.*, 2015, **28**, 16–27.
14 Y. Zhuanga, J. G. Seong and Y. M. Lee, *Prog. Polym. Sci.*, 2019, **92**, 35–88.
15 J. Ju and J.-H. Chang, *Macromol. Res.*, 2014, **22**, 549–556.
16 R. Yokota, S. Yamamoto, S. Yano, T. Sawaguchi, M. Hasegawa and R. Sato, *High Perform. Polym.*, 2001, **13**, S61–S72.
17 J. E. Han, B. K. Jeon, B. J. Goo, S. H. Cho, S. H. Kim, K. S. Lee, Y. H. Park and J. Y. Lee, *Polymer*, 2009, **33**, 91–95.
18 Y.-Y. Liu, J.-H. Cao, Y. Wang, S.-G. Shen, W.-H. Liang and D.-Y. Wu, *ACS Appl. Polym. Mater.*, 2022, **4**, 7664–7673.
19 S. K. Lim, L. Setiawan, T.-H. Bae and R. Wang, *J. Membr. Sci.*, 2016, **501**, 152–160.
20 A. Sarkar, P. N. Honkhambe, C. V. Avadhani and P. P. Wadgaonkar, *Eur. Polym. J.*, 2007, **43**, 3646–3654.
21 C. J. Cobos, A. E. Croce, K. Luther and J. Troe, *J. Phys. Chem. A*, 2010, **114**, 4755–4761.
22 N. K. Srinivasan, M.-C. Su, J. V. Michael, A. W. Jasper, S. J. Klippenstein and L. B. Harding, *J. Phys. Chem. A*, 2008, **112**, 31–37.
23 T. Matsumoto, *Macromolecules*, 1999, **32**, 4933–4939.
24 Y. Tsuda, R. Kuwahara, K. Fukuda, K. Ueno and J. M. Oh, *Polym. J.*, 2005, **37**, 126–132.
25 Y.-Y. Liu, Y.-K. Wang and D. Y. Wu, *J. Appl. Polym. Sci.*, 2022, **139**, e52604.
26 N. Saba, P. M. Tahir and M. Jawaid, *Polymers*, 2014, **6**, 2247–2273.
27 J. X. Chan, J. F. Wong, M. Petru, A. Hassan, U. Nirmal, N. Othman and R. A. Ilyas, *Polymers*, 2021, **13**, 2867–2913.
28 M. H. Nazari, Y. Zhang, A. Mahmoodi, G. Xu, J. Yu, J. Wu and X. Shi, *Prog. Org. Coat.*, 2022, **162**, 106573–110660.
29 G. Lagaly, *Appl. Clay Sci.*, 1999, **15**, 1–9.
30 K. Kwon and J.-H. Chang, *J. Compos. Mater.*, 2015, **49**, 3031–3044.
31 H. I. Shin and J.-H. Chang, *Polymers*, 2020, **12**, 135–152.
32 J. M. Garcia-Martinez, O. Laguna, S. Areso and E. P. Collar, *J. Polym. Sci., Part B: Polym. Phys.*, 2000, **38**, 1564–1574.
33 K. Yano, A. Usuki, A. Okada, T. Kurauchi and O. Kamigaito, *J. Polym. Sci., Part A: Polym. Chem.*, 1993, **31**, 2493–2498.

34 W. F. Jaynes and J. M. Bingham, *Clays Clay Miner.*, 1987, **35**, 440–448.
35 A. Ranade, N. A. D'Souza and B. Gnade, *Polymer*, 2002, **43**, 3759–3766.
36 O. Yucel, E. Unsal, J. Harvey, M. Graham, D. H. Jones and M. Cakmak, *Polymer*, 2014, **55**, 4091–4101.
37 M. Y. Choi, S. J. Lee, L. K. Kwac, H. G. Kim and J.-H. Chang, *RSC Adv.*, 2021, **11**, 30479–30486.
38 Y. D. Lee, K. Kim, Y. Ok, M. Kim and J.-H. Chang, *Polymer*, 2016, **40**, 298–305.
39 W. Li, X. Qian, H. Shi, W. Zhou, Y. Cai, Y. Liu and K. Shen, *J. Polym. Sci., Part A: Polym. Chem.*, 2017, **55**, 3243–3252.
40 K. Kim, T. Yoo, J. Lee, M. Kim, S. Lee, G. Kim, J. Kim, P. Han and H. Han, *Prog. Org. Coat.*, 2017, **112**, 37–43.
41 K. Kawasaki, T. Ebina, F. Mizukami, H. Tsuda and K. Motegi, *Appl. Clay Sci.*, 2010, **48**, 111–116.
42 D. L. Pavia, G. M. Lampman, G. S. Kriz and J. A. Vyvyan, *Introduction to Spectroscopy*, Cengage Learning, Boston, Massachusetts, USA, 2008, Ch. 2, pp. 14–95.
43 D. L. Pavia, G. M. Lampman, G. S. Kriz and J. A. Vyvyan, *Introduction to Spectroscopy*, Cengage Learning, Boston, Massachusetts, USA, 2008, Ch. 4, pp. 146–183.
44 H. H. Murray, *Appl. Clay Sci.*, 1991, **5**, 379–395.
45 D. Porter, E. Metcalfe and M. J. K. Thomas, *Fire Mater.*, 2000, **24**, 45–52.
46 R. A. Vaia and E. P. Giannelis, *Macromolecules*, 1997, **30**, 8000–8009.
47 A. B. Morgan and J. W. Gilman, *J. Appl. Polym. Sci.*, 2003, **87**, 1329–1338.
48 T. Agag and T. Takeichi, *Polymer*, 2000, **41**, 7083–7090.
49 H. Xu, S.-W. Kuo, J.-S. Lee and F.-C. Chang, *Macromolecues*, 2002, **35**, 8788–8793.
50 J.-H. Chang, B.-S. Seo and D.-H. Hwang, *Polymer*, 2002, **43**, 2969–2974.
51 Y. Na, L. K. Kwac, H. G. Kim, Y. L. Joo and J.-H. Chang, *RSC Adv.*, 2023, **13**, 16285–16292.
52 O. Becker, R. J. Varley and G. P. Simon, *Eur. Polym. J.*, 2004, **40**, 187–195.
53 J. Zhu, F. M. Uhl, A. B. Morgan and C. A. Wilkie, *Chem. Mater.*, 2001, **13**, 4649–4654.
54 J. Isac-García, J. A. Dobado, F. G. Calvo-Flores and H. Martínez-García, *Experimental Organic Chemistry*, Academic press, New York, USA, 2016, Ch. 9, pp. 291–352.
55 U. Min, J.-C. Kim and J.-H. Chang, *Polym. Eng. Sci.*, 2011, **51**, 2143–2150.
56 F. Liu, Z. Liu, S. Gao, Q. You, L. Zou, J. Chen, J. Liu and X. Liu, *RSC Adv.*, 2008, **8**, 19034–19040.
57 K. Yano, A. Usuki and A. Okada, *J. Polym. Sci., Part A: Polym. Chem.*, 1997, **35**, 2289–2294.
58 S. Sequeira, D. V. Evtuguin and I. Portugal, *Polym. Compos.*, 2009, **30**, 1275–1282.
59 C.-P. Yang and Y.-Y. Su, *Polymer*, 2005, **46**, 5778–5788.